The Breakdown and Surface Characteristics of Polymer Interfaces Under HV Impulses

Timothy Wong, *Graduate Student Member, IEEE*, Igor Timoshkin, *Senior Member, IEEE*, Scott MacGregor, *Senior Member, IEEE*, Mark Wilson, *Member, IEEE*, Martin Given, *Senior Member, IEEE*

***Abstract*—With the ever-increasing requirements placed on current and future pulsed power systems in terms of voltage, power, and compactness; solid insulation is a strong candidate for the development of novel insulation systems capable of meeting these specifications. However, the issue of solid-solid interfaces under non-standard and fast-rising impulses must firstly be addressed, as the failure to do so may pose significant risk of electrical breakdown due to reduced dielectric strength across interfacial contacts. In this work, the impulsive breakdown characteristics across dry-mate solid interfaces formed between PVC (polyvinylchloride), Torlon (polyamide-imide), Delrin (polyoxymethylene), Perspex (polymethylmethacrylate), and Ultem (polyetherimide) has been investigated in atmospheric air and under two different impulsive waveforms rising at ∼2400 kV/µs and ∼0.35 kV/µs. The statistical treatment of the obtained impulsive breakdown voltages and time to breakdowns are presented, alongside an analysis of the post-breakdown surfaces and discharge channel morphologies. The results indicate that under low mating pressure conditions (10's of kPa), the interfacial breakdown strength may be below that of only an air gap with no dielectrics. A correlation between the estimated asperity aspect ratio and the interfacial breakdown strength has been observed. This suggests that under the present experimental conditions, field enhancement around surface asperities may be a dominating factor which defines the breakdown strength of the interface, since the surface asperities do not deform sufficiently to form strong interfacial contact spots, and thus reducing the interfacial tracking resistance. This therefore provides little to impede the development of interfacial discharges. The widths of post-breakdown traces left by plasma channels on the contacting surfaces have also been shown to be dependent on the rate of voltage rise, *dV/dt*, and on the material forming the interface. The results arising from this work may aid in the future development of high voltage solid insulating systems for power and pulsed power systems.**

***Index Terms*—solid-solid interfaces, dielectric phenomena, electrical insulation, pulsed power, electrical breakdown**

I. Introduction

In recent decades, numerous novel technologies operating under the principles of pulsed power have been developed, with wide-ranging impacts to a vast array of industries. Successful application of pulsed power technology has benefited the food processing [1], [2], environmental [3], [4], and manufacturing industries [5]; while pulsed power research continues to contribute a significant amount of critical design knowledge towards the power [6], aerospace [7], and defense [8] sectors. No matter the application, reliable operation of pulsed power systems is underpinned by electrical insulation.

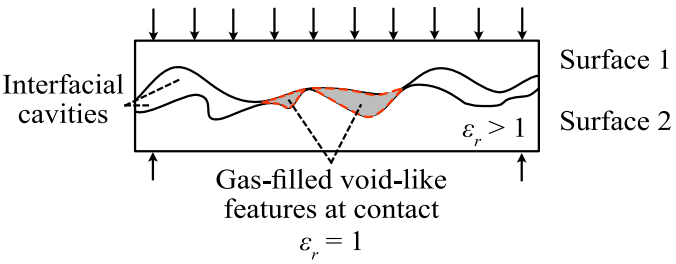

Fig. 1. Graphical depiction of gas-filled, void-like features formed between two solid surfaces at a solid-solid interface. The lower permittivity of the gas leads to field enhancement.

The continuing advancement of pulsed power systems has led to increasing levels of transient electrical stress being placed on insulating components, resulting from the need for miniaturization and from increases in operational voltage and power. Solid insulation offers unparalleled dielectric performance in comparison to liquid or gas, and has become an attractive option to support system miniaturization. For some applications, all-solid insulation systems [9] have been proposed and are seen as a possible method to push system specifications higher than ever before. However, to successfully integrate solid insulation into pulsed power systems, points of potential weakness must first be identified and addressed.

One such weakness is the inevitable formation of solid-solid interfaces – contacts between separate solid insulators most often found at connections or joints. Breakdown across solid interfaces is well known to occur at far lower voltage stresses than in bulk solids [10]–[12]. The conclusions of multiple studies [9], [13]–[15] indicated that the mechanism of solid interfacial weakness may be driven by gas breakdown inside the void-like features developed at the contacting surfaces. These features result from the inherent and unavoidable surface roughness of the materials forming the connection, whereby cavities on the solid dielectric surfaces form gas-filled voids along the interfacial contact, as illustrated in Figure 1. In a series of studies, Kantar *et al.* [16]–[19] tested this idea further, successfully correlating the surface roughness [17], elastic modulus [18], [19], and contact pressure [17] to the

T. Wong was supported in part by the Engineering and Physical Science Research Council (EPSRC) under grant number EP/T517938/1.

Manuscript received Month XX, 2024; revised Month XX, 2024.

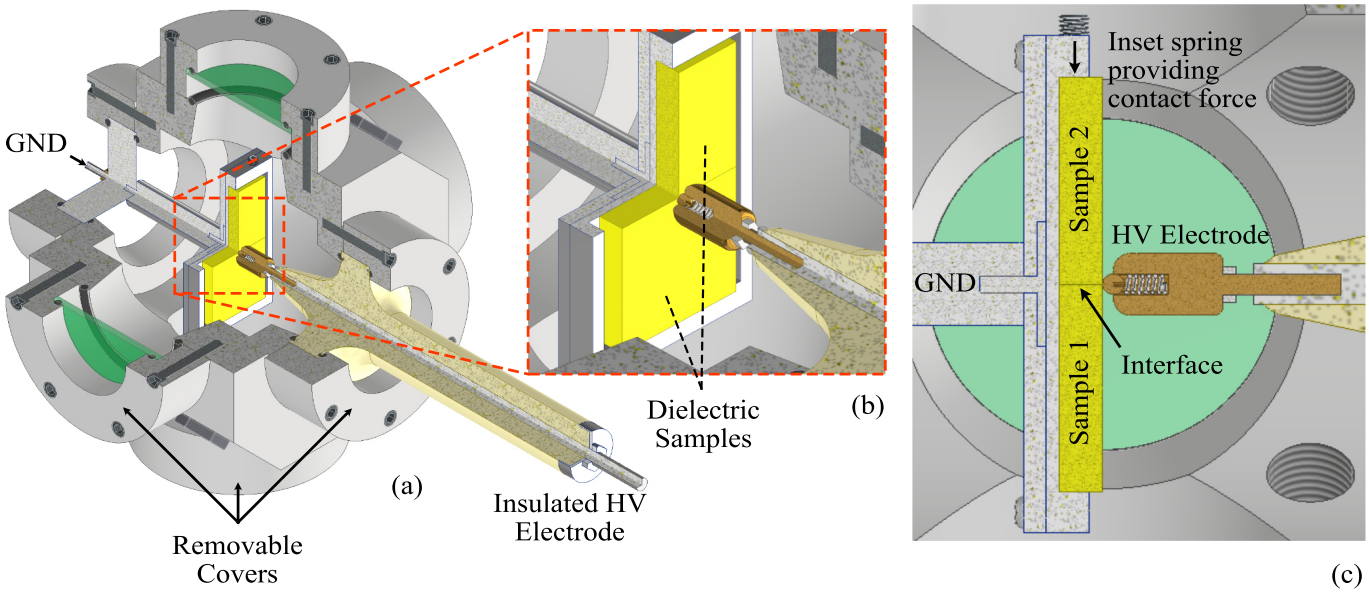

Fig. 2. (a) 3/4 cutaway view of a 3D model of the utilized test chamber, (b) magnified image showing the location of the solid samples forming the solid interface, and the spring loaded HV electrode, (c) sectional view through the center of the soid sample holder, indicating the locations of the inset springs providing the sample holding force.

interfacial breakdown strength under AC electrical stress at power frequencies. The authors further conducted comprehensive modelling work [20], [21] which supported these findings. The culmination of these works has raised awareness for the need to consider the mechanical and tribological properties of solid interfaces when designing solid insulation systems.

In general, however, there is a lack of both experimental characterization and theoretical exploration of solid interfaces under impulsive breakdown and for pulsed applications. This includes fast-rising non-standard impulsive stress, nonuniform field geometries, and atypical materials outside of those common to power equipment. The objective of the present work is to begin the expansion of solid interface characterization to the impulsive regime, by experimentally investigating the impulsive breakdown characteristics of solid interfaces formed between five materials: PVC (polyvinylchloride), Torlon (polyamide-imide, also known as Duratron T4203), Delrin (polyoxymethylene), Perspex (polymethylmethacrylate), and Ultem (polyetherimide, also known as Duratron U1000). This work focuses on the breakdown voltage and time to breakdown of solid-solid interfaces (with both sides formed of the same material – non-matching interfaces have been left as a subject for future work) stressed with HV impulses with different rates of rise (*dV/dt*), and on the analysis of the post-breakdown morphological changes on the surfaces induced by spark plasma channels.

II. Experimental Methodology

A. Test Chamber and Circuit

Breakdown testing on the material samples were conducted using the test cell shown in Figure 2. The sealed main chamber housed a custom-designed sample holder which could accommodate two 50 by 50 mm square material samples, held in contact by two spring-loaded ball bearings fitted inside the holder edge. The contact pressure at the interface was therefore kept consistent via the downforce exerted by the deformation of the spring, estimated in the range of 10's of kPa based on the measured spring constant and deformation distance. The assembled holder was placed inside the sealed chamber, where an adjustable brass ball bearing electrode of radius r = 3.5 mm was positioned in contact with the interface formed between the two samples. The base of the sample holder therefore acted as the ground (plane) electrode. The chamber can be pressurized with different gases; however, the present work focused only on breakdown at atmospheric pressure in laboratory air. The chamber was evacuated after each breakdown shot using a vacuum pump and filled with fresh air, ensuring identical gas conditions were present for each data point.

The circuit diagram of the test circuit is shown in Figure 3. The configuration consisted of a high voltage (HV) impulse generator connected to the HV electrode, which was either a custom-built stacked Blumlein generator following the topology shown in [22] charged at 30 kV using a Glassman HV power supply through a 1 MΩ charging resistor and with a nominal multiplication factor of 4, or a Samtech TG-01 generator with a peak voltage output of 35 kV. The former was used to generate impulses of ∼50 ns rise time (∼2400 kV/µs) by triggering the pulse using a self-breaking spark gap, and the latter to generate longer, ∼100 µs rise time impulses (∼0.35 kV/µs). Voltage monitoring was provided through a copper sulphate (CuSO4) divider (1:8) and a Northstar PVM-5 HV probe (1:1000, 80 MHz nominal bandwidth), while the current signal was recorded using a Pearson model 6600 current monitor (0.1 V/A, useful rise-time 5 ns). Breakdown voltage and current signals were captured simultaneously on a Textronix TDS3045C digital oscilloscope (500 MHz bandwidth, 5 GS/s).

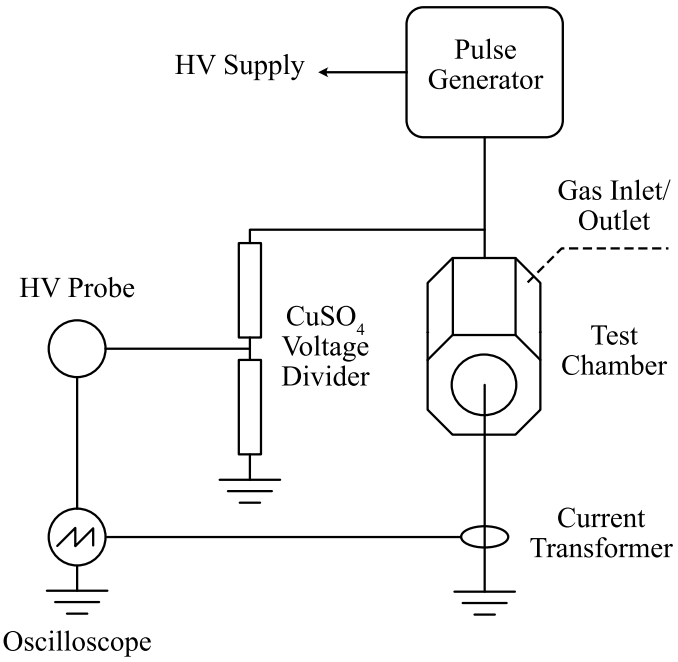

Fig. 3. Circuit diagram of the experimental test circuit. The pulse generator was either a custom-built stacked Blumlein [22] triggered using a self-breaking spark gap, or a Samtech TG-01 pulse generator. In the latter case, the $CuSO_4$ voltage divider was not necessary due to the lower peak voltage.

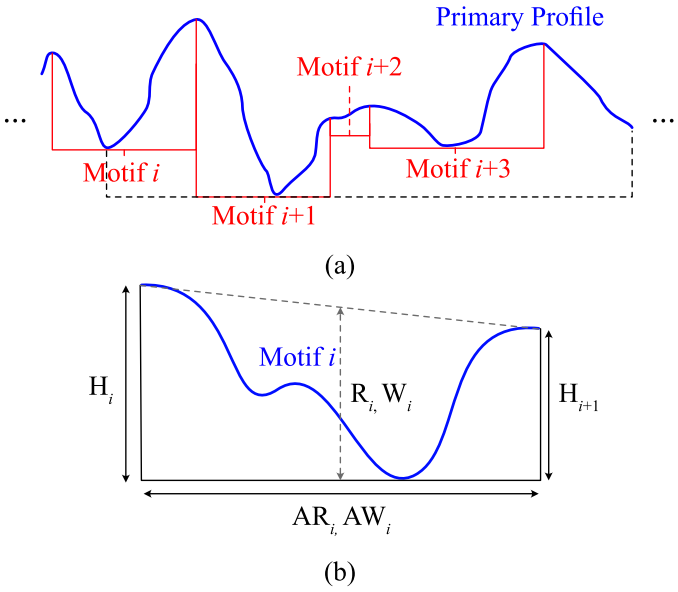

Fig. 4. Example of (a) motif profile that can be extracted from the primary surface profile of a rough surface, made up of a chained number of motifs, (b) depiction of a single motif, labelled with relevant parameters described in Table II.

B. Material Samples

Sheets of PVC, Delrin, Torlon, Perspex, and Ultem were cut into 50 by 50 mm square samples. An identical cutting process was following for all four edges of each sample, to ensure that the surfaces would be treated consistently for each material. Consistency was confirmed using roughness measurements as described in section II-C. As this study did not aim to focus on varying the surface roughness, no additional treatment of the cut surfaces was performed. It is remarked that by using the freshly cut samples 'as received' is perhaps more representative of the level of surface treatment used in most practical industrial use cases, as surface treatment to attain specific surface conditions would not be performed for most standard applications. Roughness characterization of the cut surface, however, was conducted following the methodology of section II-C. Table I includes other relevant properties of each material used in this work.

TABLE I
RELEVANT PROPERTIES FOR THE MATERIALS INVESTIGATED IN THIS WORK.

Material	Thickness d_s, mm	Relative Permittivity, ε_r	Elastic Modulus E, MPa
PVC	12.14	2.9	3400
Delrin	10.72	3.7	2800
Torlon	10.33	3.9	4200
Perspex	9.44	3.6	3200
Ultem	13.25	3.0	3500

C. Surface Roughness Characterization

In accordance with the past findings of gas cavity driven interfacial breakdown, it is known that the roughness conditions of the contacting surfaces can play a major role in the determination of interfacial breakdown strength [17]. Thus, all surfaces used in this work were also subjected to surface characterization prior to breakdown testing.

To do so, surface profiles at four evenly-spaced intervals across each material sample were taken prior to breakdown tests, using the Accretech "Handysurf 35+" profilometer with an evaluation length of 5 mm. The instrument features a diamond-tipped mechanical stylus of 2 µm tip radius, and although the profilometry method is mechanical in nature, the downward stylus force of only 0.75 mN (estimated pressure ~60 MPa) was sufficiently small to not inscribe any of the contact surfaces, and therefore would not affect the breakdown results. The motif method as prescribed by the ISO12085 standard [23] (and also used in [20]) was used to process the measured primary roughness profiles, allowing the extraction of the roughness and waviness characteristics of the surfaces under test. The details of the method are well documented elsewhere [20], [23] and so only a brief outline of the process and relevant outputs are provided below.

With reference to Figure 4, the motif method can extract the so-called motif profiles of the primary profile curve, separating the short-wavelength (roughness motif) variations from the long-wavelength (waviness motif) features of the primary roughness curve. The motifs of the surface can be used to calculate several relevant surface parameters, as tabulated in Table II. Knowledge of these surface parameters enables the application the equivalent surface method [24] for surface contact, and so the equivalent surface parameters for an interface between surface 1 and surface 2 can be calculated

as:

$$\begin{aligned} R_{eq} &= R_1 + R_2 \\ W_{eq} &= W_1 + W_2 \\ AR_{eq} &= \frac{1}{2}\left(AR_1 + AR_2\right) \\ SR_{eq} &= \sqrt{SR_1^2 + SR_2^2} \\ SW_{eq} &= \sqrt{SW_1^2 + SW_2^2} \\ SAR_{eq} &= \sqrt{SAR_2^2 + SAR_2^2} \end{aligned} \tag{1}$$

where the parameters with subscripts 1 and 2 correspond to the first and second surfaces in contact, and subscript *eq* describe the properties of the combined two-surface contact as the contact of an equivalent surface against an ideally flat plane. In this work, the equivalent surface parameters were calculated from the averaged parameters of the contacting surfaces over the four measurement locations. In this way, a quantitative measure of the surface roughness condition of each solid interface could be made, and which is included within the analyses presented in section IV.

D. Experimental Procedure

Sample preparation involved firstly taking surface roughness measurements of the sample surfaces, following section II-C. Each surface was then cleaned using a 70% ethanol-water solution and with low-lint paper, with care taken to remove any residue or other foreign material that may become caught between the surfaces when the contact is made. The holder with dried and assembled samples was then secured, with the HV electrode positioned such that it would be in light contact with the samples, before the chamber was sealed.

Each interface (formed between one pair of samples) was subjected to 20 HV shots, with a 1 min 30 s delay between each shot to ensure that any residual charges could fully dissipate. This was confirmed using a Trek 347 electrostatic voltmeter during initial tests, which saw the surface potential drop to negligible levels rapidly after interfacial discharge. During this time, the test chamber was also flushed and replaced with fresh air. As the stored energy for either of the pulse generation systems used in this work was quite low, 20 shots could be applied to one interface without significant surface damage, avoiding any skewing of the breakdown results with shot number.

TABLE II
MOTIF PARAMETERS COMPUTABLE FROM ROUGHNESS AND WAVINESS MOTIF PROFILES ACCORDING TO [20], [23]. NOTE THAT THE SUBSCRIPT i USED HERE IDENTIFIES THE i-TH MOTIF ALONG THE ANALYZED SURFACE.

Parameter	Description
R	Average roughness motif heigh across all R_i.
W	Average waviness motif height across all W_i.
AR	Average roughness motif widths across all AR_i.
SR	Root-mean-square of roughness motif heights across all R_i.
SW	Root-mean-sqaure of all waviness and motif heights across all W_i.
SAR	Root-mean-square of all roughness motif widths across all AR_i.

For each polarity, a total of 40 shots were applied to two different interfaces. This was done to ensure that the breakdown characteristics would largely be the same for an interface of the same material. Though, it should be noted that the first 20 shots on the first interface cannot be directly compared to the second 20 shots on the second interface, since their surface roughness characteristics would not be identical. Thus, the distinction between the first 20 and second 20 shots for each material-polarity pair is also maintained within the results section IV.

III. PROCESSING AND STATISTICAL TREATMENT OF BREAKDOWN DATA

Using the instrumentation described in section II-A, voltage breakdown waveforms were recorded for each shot. Examples of typical raw signals attained from the 2400 kV/μs and 0.35 kV/μs cases are shown in Figure 5(a) and 5(b), respectively. To extract the value of breakdown voltage from each waveform, raw signals (as shown in Figure 5) were first filtered using a simple moving-average, which helps to reject noise and oscillations around the peak. A filter window length of 10 was used in all cases, corresponding to low-pass cut-off frequencies of approximately 200 MHz and 2 MHz for the 2400 kV/μs and 0.35 kV/μs signals, respectively. The peak position of the smoothed waveform then becomes unambiguous and was taken to be the breakdown voltage. The corresponding time between the beginning of the voltage rise (first zero-crossing of the waveform) and the peak voltage was recorded as the time to breakdown. This process is effectively an algorithmic and fully reproducible method of implementing visual averaging as often done for breakdown waveforms. Note that the output of the algorithm for every waveform was also subjected to manual inspection to ensure that the correct points were identified.

The 20 breakdown voltage and time to breakdown data-points per dataset were fit to two-parameter Weibull distributions (where it is assumed that the formative time is effectively zero in comparison to the statistical time lag), informed by both Kolmogorov-Smirnov and Lilliefors goodness-of-fit tests at 95% confidence. The probability distribution function (PDF) is therefore of the form:

$$f(p;\alpha,\beta) = \frac{\beta}{\alpha}\left(\frac{p}{\alpha}\right)^{\beta-1}\exp\left[\left(-\frac{p}{\alpha}\right)^{\beta}\right] \tag{2}$$

where p is either voltage or time, α is the scale parameter, and β is the dimensionless shape parameter. The fitting was conducted using the maximum likelihood estimation (MLE) method, which seeks the maximization of the log-likelihood function L:

$$L = \prod_{i=1}^{n} f_i\left(p_i, \hat{\theta}\right) \tag{3}$$

$$\frac{d\log L}{d\hat{\theta}} = 0 \tag{4}$$

where $\hat{\theta}$ are the optimal parameters $\hat{\alpha}$ and $\hat{\beta}$ that maximize the likelihood function with the number of observations n, thereby describing the best-fitting distribution and enabling the Confidence Intervals (CIs) to be computed. In the present

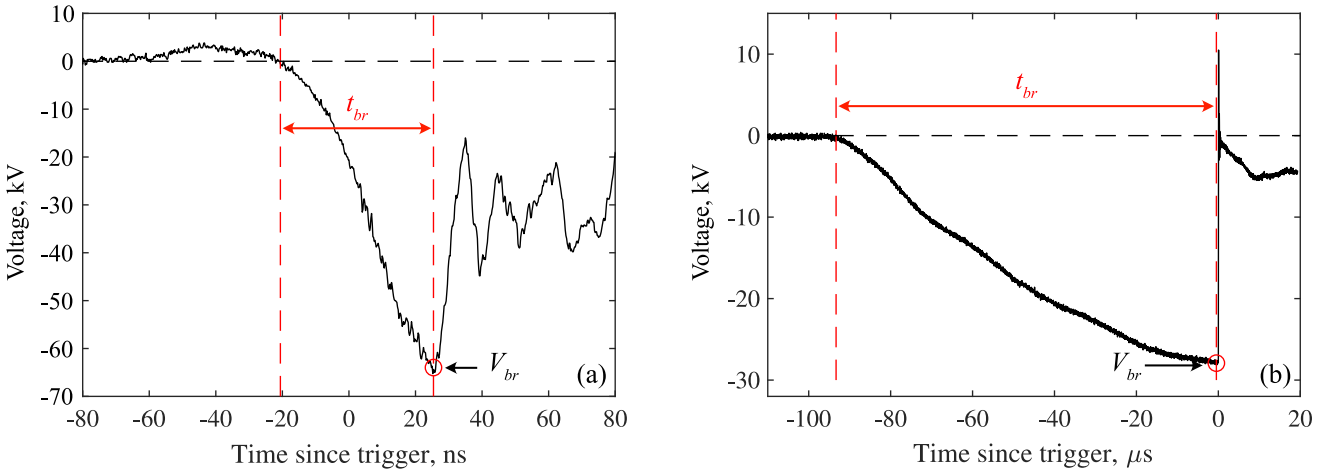

Fig. 5. Oscillograms of typical voltages obtained during breakdown for (a) 50 ns rise time stacked-Blumlein, (b) 100 µs rise time Samtech TG-01 pulse generator. Red circle indicated the identified breakdown voltages, red dashed lines show the identified time to breakdown.

context, $\hat{\alpha}$ is equal to the voltage or time at which 63.2% of samples had failed, which is taken to be the characteristic breakdown voltage or time of the interface ($\hat{\alpha} = V_{br}$ or $\hat{\alpha} = t_{br}$, depending on the dataset). It is remarked that a comparison was made between the MLE method and the commonly used least-squares (LSQ) linear fitting and median ranks approximation, finding that MLE was generally superior at outlier rejection for the data handled in this work. For data that had no outliers, the LSQ and MLE methods provided essentially identical fittings. To compensate for the varying thicknesses (see Table I) of the different materials, a nominal average breakdown field value, E_{br}, was calculated from each obtained breakdown voltage following $E_{br} = V_{63.2}/d_s$, where d_s is the sample thickness (equal to the minimum interelectrode gap distance). This value is used as a means of comparison between different materials in section IV-A as an indicator for the interfacial breakdown strength.

IV. Results and Discussion

A. Impulse Breakdown Strength and Material Choice

Figure 6 shows E_{br} and $t_{63.2}$ with 95% CIs for the 2400 kV/µs and 0.35 kV/µs cases, and for all material-polarity pairs. Dashed and dash-dot lines further show E_{br} in absence of any solid interface at 10 mm separation for negative and positive polarities, respectively. Note that in the specific electrode configuration used here, the 2400 kV/µs case saw almost identical negative and positive breakdown voltages in the no-solid case. This suggests that the gap distance (10 mm) used for the no-solid tests in the 2400 kV/µs case is close to the critical gap distance, d_{crit}, of this electrode topology, where the breakdown strengths are the same for both polarities as described in [25]. The authors of [25] and references therein indicate that this phenomenon may be attributed to the development and transport of space charge in nonuniform fields. This explanation is supported by the observed differences in breakdown time between positive and negative impulses shown in Figure 6(c), despite near-identical breakdown voltages. Development of sufficient space charge may affect the overall *dV/dt* of the voltage across the gap nearing the moment of breakdown, leading to a difference in the time to breakdown despite the breakdown occurring at the same voltage magnitude. It is also noted that additional no-solid breakdown tests were conducted using a range of gap distances (around 10 mm, since materials were not of equal thickness), and little variance in the normalized breakdown field was found. The relative positions of E_{br} between the no-solid case and breakdown with an interface of Figure 6 would remain the same.

Believed to be resulting from the same phenomenon, positive breakdown could not be attained in the no-solid case for 0.35 kV/µs impulses, but negative breakdown occurred consistently, indicating that in this case, 10 mm may in fact be smaller than d_{crit} as defined in [25]. This suggests that d_{crit} may also be dependent on *dV/dt*. It should further be noted that upon the introduction of a solid interface, the 0.35 kV/µs case sees negative breakdown be consistently higher than positive breakdown (Figure 6(b)), but the 2400 kV/µs case remains inconclusive (Figure 6(a)). This further suggests that the existence of the solid interface may also affect the critical distance, but investigation of this phenomenon is left as a subject for future work.

Based on Figures 6(a) and 6(b), it has been observed that the impulsive breakdown strengths of the solid interfaces are not only vastly inferior to that of bulk solids (typically in the range of MV/cm, e.g., [26], [27], but in the majority of cases reduced the system breakdown strength to significantly below that of just air alone. In [16], authors have suggested that the tracking resistance of the interfacial contact spots may be important to determine the total breakdown strength of a solid interface. This was under the consideration that the interfacial voids which partially discharge must subsequently be chained together via breakdown of the contact spots, leading to full interfacial breakdown. In this work, the low interfacial mating pressure (∼10's kPa) is believed to have the equivalent effect of significantly reducing the contact-spot tracking strength. In this way, it is theorized that under these conditions, the

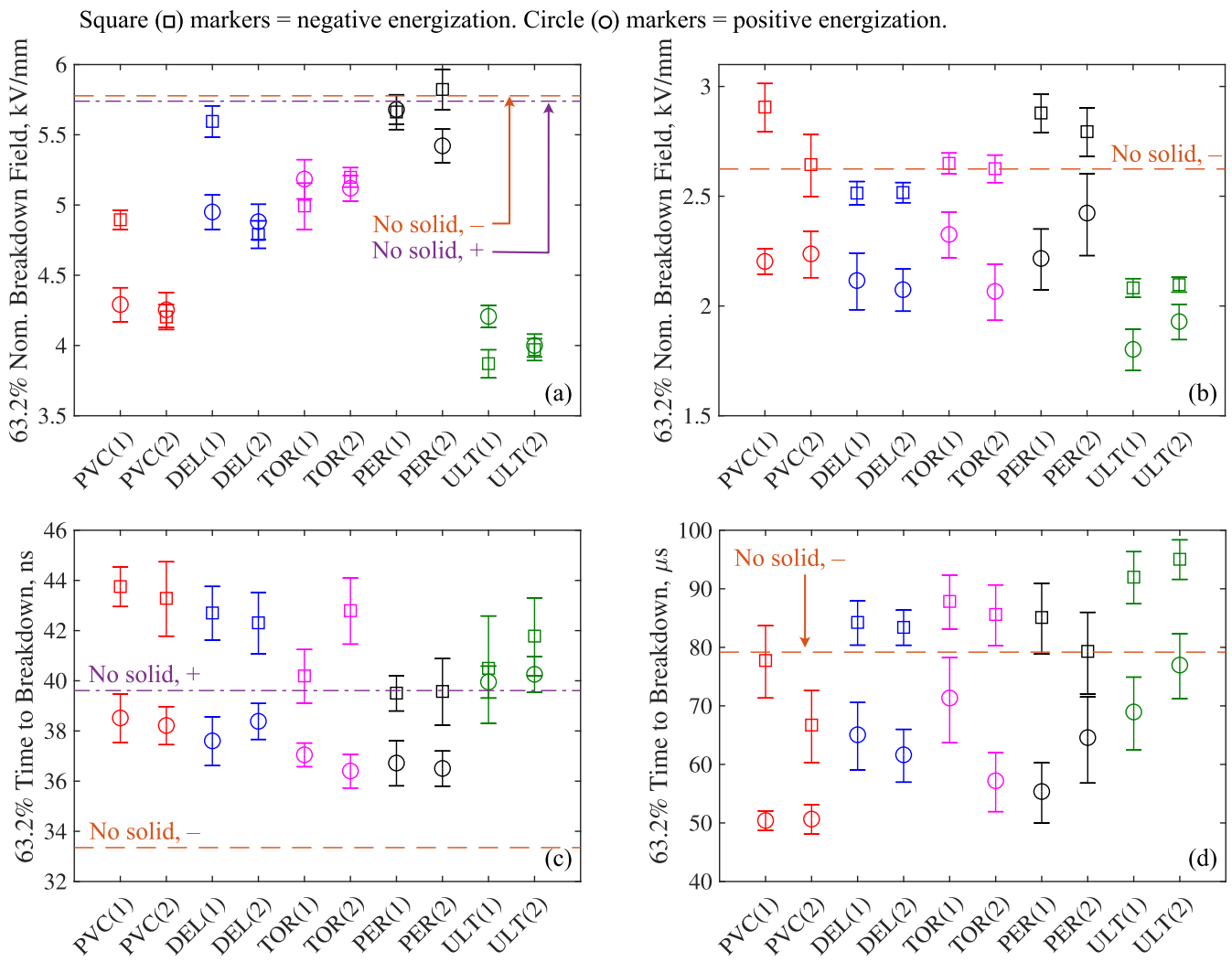

Fig. 6. Nominal breakdown fields, E_{br}, for all materials and both polarities in the (a) 2400 kV/μs case, (b) 0.35 kV/μs case. Time to breakdown, $t_{63.2}$, for all materials and both polarities in the (c) 2400 kV/μs case, (d) 0.35 kV/μs case. Orange and purple dash-dot lines indicate the corresponding E_{br} and $t_{63.2}$ values in the case of an air gap with no solid included. These are absent for positive polarity in figures (b) and (d) since breakdown did not occur. Error bars show the 95% confidence intervals.

interfacial contact spots do very little to obstruct the evolution of the breakdown across the length of the interface. Initial discharges which form within the interfacial voids (due to the enhancement of the electric field inside them) can readily chain together, such that the breakdown strength of the interfacial voids alone essentially determines the breakdown strength of the whole interface. Now considering that the electric field is enhanced due to dielectric polarization inside the voids (and therefore for the same voltage stress, the field will be higher at the solid interface than in the no-solid case), it explains the observed reduction of the interfacial breakdown strength below that of just air under the same electrode and voltage conditions. This may be a critical design issue for insulation systems which incorporate solid interfaces, showing that a loss of interfacial pressure may result in the reduction of the system breakdown strength to below that of solely gas insulation.

When comparing across materials, one should do so with caution as the surface roughness conditions even between the same materials may not be identical. However, the breakdown results of Figure 6 are reasonably consistent for interfaces of the same material, suggesting that the surface morphologies were also of fair consistency between samples. Since the resulting surface condition after cutting is also a characteristic of the material itself, it would therefore not be unreasonable to draw some form of a comparison. Considering the 95% CIs (and across breakdown results of the same polarity), PVC, Delrin, and Torlon interfaces appeared to have similar breakdown strengths and time to breakdowns in the 0.35 kV/μs case. For the 2400 kV/μs case, Delrin and Torlon interfaces remain similar, with PVC falling below by approximately 1 kV/mm in nominal breakdown field for three out of four tests. Perspex interfaces could be considered the highest performing of the materials tested, with a higher nominal breakdown strength in most cases. Most notably, however, is that Ultem interfaces were significantly weaker than those formed by all other materials. A difference of ∼2 kV/mm compared to Perspex interfaces was observed in the 2400 kV/μs case, and ∼1 kV/mm in the 0.35 kV/μs case. Inspection of the raw

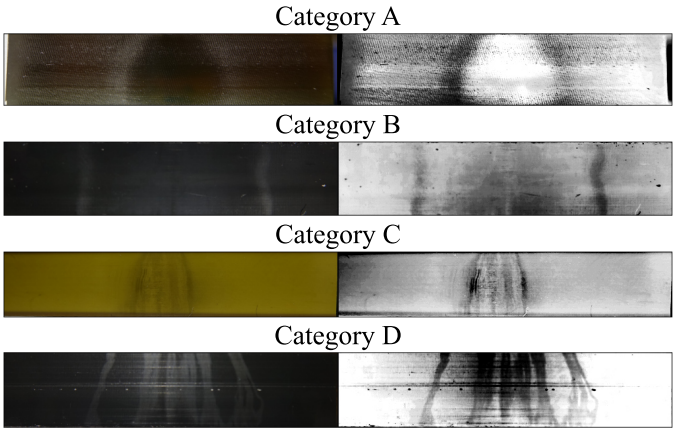

Fig. 7. The four identified categories of post-breakdown traces left on the contacting sample surfaces. Descriptions given in the main text. Left images show photographs, right images are contrast and brightness adjusted greyscale versions for clarity.

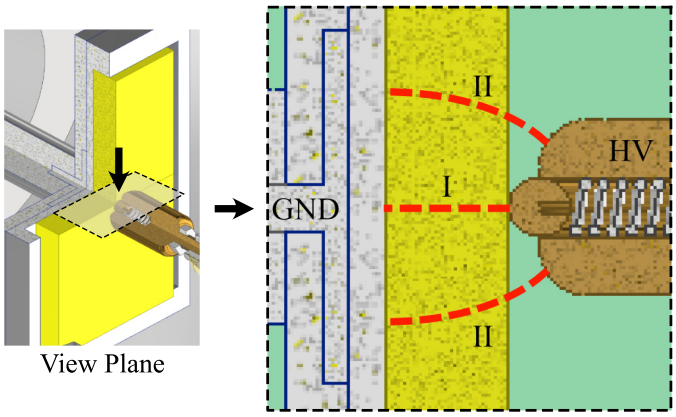

Fig. 8. Magnified image of the contact point between the HV electrode and interface. Breakdown path labelled I corresponds to cases A and B, while paths labelled II delineates the longer path taken (through the gas first) as in cases C and D.

values of $V_{63.2}$ rather than nominal fields indicated that Ultem interfaces possessed similar breakdown voltages to all other materials, despite being almost 4 mm thicker in compared to the thinnest materials.

For the 2400 kV/µs case, the primary cause of this ranking is believed to be the differences in sample thickness. A direct correlation between the sample thicknesses of Table II and E_{br} can be seen, where a thicker sample resulted in a lower value for E_{br}, despite being normalized by the gap distance. It is believed that the most important factor here is the *rate of change of field*, dE/dt, rather than the applied dV/dt. The developed field for thinner samples at a certain fixed value of dV/dt will rise with a greater value of dE/dt, which likely results in higher E_{br} based on the typical behavior of gas breakdown in the present overstressed impulsive regime. Considering that the interfacial breakdown is determined by intra-cavity gas discharge, the results would suggest that the increased E_{br} of thinner interfaces due to the effects of greater dE/dt is dominant over any corresponding reduction of E_{br} resulting from decreased d_s. This observation, however, is not entirely clear for the 0.35 kV/µs case, suggesting that the above is only a partial explanation. In both cases, Ultem was also observed to possess a far lower E_{br} compared to other materials, even when accounting for the greater thickness. It is believed that the surface roughness characteristics of Ultem may provide a secondary process which explains this observation, and is discussed in more details within section IV-E.

B. Post-breakdown Surfaces and Discharge Channel Morphology

The low energy output of both generators used in this work meant that no significant surface damage was induced by repeated breakdown in terms of burning or drastic modification of the surface texture. However, the discharge plasma channels leave visible marks across the interface which show the discharge path(s) taken over the 20 breakdown shots. Only PVC and Torlon exhibited (light) carbonization, and only for positive 2400 kV/µs impulses. Figure 7 shows several examples of the surfaces photographed after testing. Considering all experiments that were conducted, four separate cases could be identified based on the shape, number, and size of the visible traces on the post-breakdown surfaces, listed below:

A) Central plasma channel with a small region of expansion. Indicates that the discharge paths were focused down the line of maximum (Laplacian) field for all 20 shots applied to the interface.
B) One single, central, plasma channel; but the expansion region was significantly wider (two to three times the width) than those in (A).
C) Multiple plasma channels originate from the spherical HV electrode, that branch across the interface following the Laplacian field lines. Indicates that the repeated discharges did not follow the same path over the multiple shots.
D) Multiple plasma channels bridge the gap as in (C); however, some channels originate not from the spherical HV electrode, but from the electrode edges (see Figure 8). Indicates that some shots took a far longer discharge path to bridge the interface that did not necessarily align with the critical path based on the Laplacian field.

With the post-breakdown trace definitions above, along with the breakdown results of Figure 6, the analyses and discussion of observations are presented in sections IV-C to IV-E.

C. Effects of Voltage Polarity

For the 0.35 kV/µs case (Figure 6(b)), the negative nominal breakdown fields were consistently higher than that of positive polarity for all materials by a statistically significant margin. This appears consistent with the theory of gas-cavity discharge driven interfacial breakdown, though clearly indicates that the critical distance (as discussed in section IV-A) must now be different, considering that this contrasts the results in just air. Higher negative breakdown voltages compared to positive for the same voltage magnitude is a well-known phenomenon in electronegative gases, generally attributed to negative space-charge effects and higher inception voltages for negative

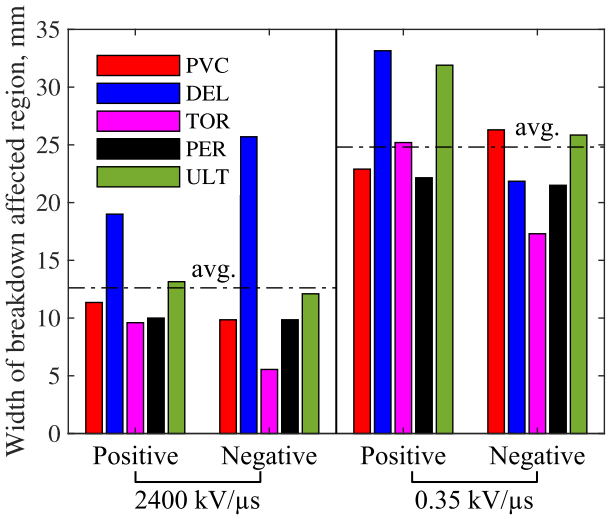

Fig. 9. The maximum width of the region affected by breakdown on the sample surfaces, after 20 shots, for both 2400 kV/µs and 0.35 µs cases. Values shown are the average width of the first and second interfaces (20 shots each).

streamers [25], but as discussed in section IV-A, applies only if the configuration is far from the critical gap distance. Comparing negative breakdown to positive breakdown for the 2400 kV/µs case (Figure 6(a)), this tendency was not observed, and the results were mixed. No notable correlations were observed between the polarity and the discharge paths for both 2400 kV/µs and 0.35 kV/µs impulses.

D. Effects of dV/dt

As is evident from Figure 6(a) and 6(b), increased breakdown voltages were recorded for the faster-rising impulse, behavior of which is consistent with the pulsed breakdown of gases alone. The same was found for all materials irrespective of polarity, attributed to the magnitude of *dV/dt* which affects the amount at which the voltage may additionally increase after the initiation of the breakdown process, and prior to voltage collapse.

The two different values of *dV/dt* used in this work also had significant effects on the paths taken by the discharges, indicated by inspection of the post-breakdown surfaces. All breakdowns induced using the 2400 kV/µs impulse had discharge paths that fell only into category A or B, and those that belonged to category B were exclusively Delrin interfaces. For the discharge paths of 0.35 kV/µs breakdown, these fell exclusively into category C or D, where category C was dominated mainly by Torlon and Perspex interfaces, and D was found for the majority PVC and Delrin interfaces. The maximum widths of the surface region affected by the breakdown (after all 20 shots) were also measured for each interface, and the average of the two values obtained was calculated for each triplet of *dV/dt*, polarity, and material. The resulting data is shown in Figure 9.

It is believed that this preference between A/B and C/D is caused by space charge effects: for lower *dV/dt*, the slower rising voltage may allow significant charge transport prior to breakdown, and space charge distortion within interfacial voids near the HV electrode tip may act to redistribute the electric field in a way that redirects the breakdown path. The degree to which the field can be distorted before discharge inception may be far lower for high *dV/dt*, and the electric field may therefore not stray far from the Laplacian field up to the time of breakdown. This may explain why multiple discharge channels were seen exclusively for the 0.35 kV/µs case, and equally explain the occurrence of case D, where the discharge path is initiated from the edge of the electrode rather than the HV tip – also only observed for 0.35 kV/µs impulses. In consequence, the average width of the affected region over all shots for the 0.35 kV/µs case was found to be approximately two times wider than that of the 2400 kV/µs case, as indicated in Figure 9 – a factor that would be even larger if Delrin would be excluded in the averaging of the 2400 kV/µs data, since it was a clear outlier in this case with the majority of Delrin traces falling into category B rather than A. Delrin, under 2400 kV/µs impulses, formed far wider regions around the central breakdown channel than all other materials. The present data suggests that this is a material-specific property, but further study which potentially explores plasma-surface interaction would have to be undertaken to confirm this, which is outside the scope of the present work.

E. Relationship with Surface Roughness Characteristics

Of the equivalent surface parameters computed following section II-C, those relevant in capturing the overall morphology of the interfaces include R_{eq}, W_{eq} and AR_{eq}, AW_{eq}, since the first two provides an indication of the degree of protrusion of surface asperities from the surface median, while the latter two gives an indication of the larger undulations of the surface profile, both of which are related to the size of the void-like gaps formed at the interface which may facilitate the discharge process.

No correlation was found directly between any of the above parameters and the nominal breakdown field. This contrasts the conclusions of past work, e.g., [17]. However, this is primarily believed to be the result of the low contact pressure used in this work. The contact pressure exerted by the holder is much lower compared to other studies (in the range of kPa rather than MPa). Each interface was held together only through a parallel spring arrangement which could easily be overcome by pushing against the samples by hand. In accordance with current theories, low mating pressure tends to increase the size of the interfacial cavities, decreases the effective contact area, and reduces the contact spot tracking resistance, hence decreasing the breakdown strength [17].

Under these conditions, however, it is believed that a different characteristic of the rough surfaces may be more impactful in determining the interfacial breakdown strength. As originally proposed in [28] and as appears in the analysis of surface asperities conducted in [29], three parameters of the equivalent surface can be used to characterize the surface roughness of the interface: the asperity density, η_{eq}, the standard deviation of the surface asperity peak heights, σ_{eq}, and the mean radius of surface asperities, β_{eq}. The latter, β_{eq}, is of interest here, which measures the average radius of surface

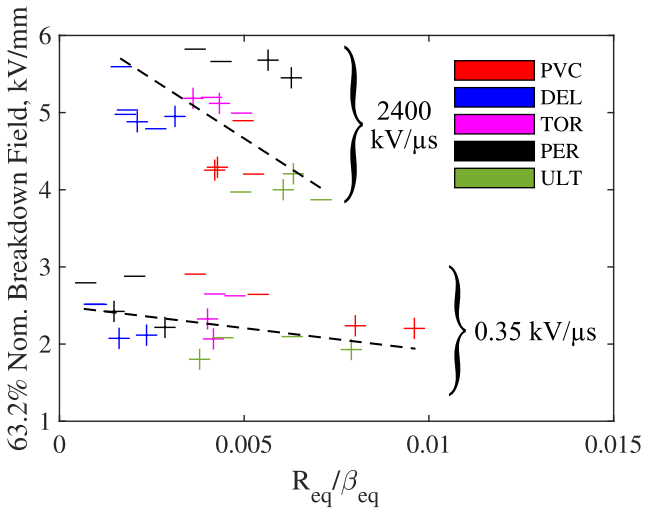

Fig. 10. E_{br} plotted against the estimated equivalent asperity aspect ratio, R_{eq}/β_{eq}, for all tested interfaces. Color shows the interface material, while the marker symbol shows polarity. Dashed black lines indicate the tendency for surfaces with higher aspect ratio asperities to result in lower breakdown strength.

asperities at the solid interface. Following the work of [29], β_{eq} can be estimated from the equivalent surface parameters given by equations (1), following:

$$\beta_{eq} = \frac{AR_{eq}^2 + SAR_{eq}^2}{16R_{eq}} \tag{5}$$

The ratio between the mean motif height (R_{eq}) and the mean asperity radius (β_{eq}) is hereby used as an indication of the *aspect ratio*, R_{eq}/β_{eq} , of the equivalent surface asperity. This dimensionless ratio can be used as a measure of the 'sharpness' of the asperity, as it provides an indication of the width of an asperity compared to its height. Figure 10 plots the nominal breakdown strength for all material-polarity pairs against R_{eq}/β_{eq} , where a negative correlation was found for both 2400 kV/µs and 0.35 kV/µs cases. Since a higher value of R_{eq}/β_{eq} corresponds to smaller and sharper asperity peaks, it is believed that the higher aspect ratio of these surface features increases the degree of local field enhancement at the interface. Coupled with the low contact pressure and consequent low tracking resistance, may possibly play a significant role in interfacial breakdown under the conditions studied here. This is in contrast to studies conducted under high mating pressure, wherein many more of these high-aspect ratio asperities may be deformed and themselves become the interfacial contact spots, acting to increase the overall interfacial breakdown strength by means of increasing the tracking resistance.

The significantly lower breakdown strength of Ultem interfaces is believed to be partially explained by the asperity aspect ratio, which in general is higher for Ultem than the other materials (Figure 6(a-b)). This is further evidenced by the visual inspection of the Ultem surfaces, which show faint diagonal serrations left behind by the cutting tool used to treat the dielectric samples – contrasting that of all the other materials where these serrations were not as evident. Considering that all materials were cut using the same tool and procedure, this suggested that there exist some mechanical property of Ultem that determines the surface condition when subjected to machining action, and as a consequence, tended to leave sharper features on Ultem surfaces. One possibility is the material brittleness: materials which are more brittle would be far more likely to exhibit local brittle fracture during machining from the impact of the cutting tool. Brittleness is typically inferred from the stress-strain curve of a material, the measurement of which was not performed in the present work. However, the brittleness of a material is known to be related to its impact strength, often measured using the Charpy impact test (ISO 179 [30]) and reported in specification sheets. The impact strength is typically provided as a single numerical value with units kJ/m2, a measure of energy absorption during fracture. Lower impact strength generally suggests that the material is brittle rather than ductile. For the materials involved here, PVC, Delrin, Torlon, and Perspex have Charpy impact strengths between 10 kJ/m^2 and 14 kJ/m^2; while for Ultem, it is significantly lower at just 3.5 kJ/m^2. This would support the hypothesis that Ultem may be more brittle than the other materials, leading to sharper surface asperities after machining due to local brittle fracture, resulting in the observed lowering of the interfacial breakdown strength. It is however clear from Figure 10 that the asperity aspect ratio is unlikely to be the only determinator of solid interfacial breakdown. More detailed modeling work is planned to be conducted to gain further understanding of other aspects that may influence the impulsive interfacial breakdown strength.

V. Conclusions and Outlook

In the present work, the impulsive breakdown characteristics of solid-solid interfaces (of matching materials) formed between PVC, Delrin, Torlon, Perspex, and Ultem have been investigated. Breakdown tests using a sphere-plane electrode configuration were conducted in laboratory air under atmospheric pressure using two different pulse generators, to obtain results under two different *dV/dt* values of approximately 2400 kV/µs and 0.35 kV/µs. Analyses on the breakdown strength and time to breakdown were performed using Weibull statistics, complemented with roughness characterization data obtained from the measurement of the pre-breakdown surface profiles of the material samples. Inspection and categorization of the nature of the post-breakdown surface traces has also been conducted. A summary of observations and conclusions that have arisen from this work is provided below:

- Solid interfaces at low mating pressure acted to reduce the impulsive breakdown strength of the system to lower than that of just air in almost all cases.
- The above point is believed to be a result of intra-cavity field enhancement at the interface, combined with significantly reduced tracking resistance due to low contact force.
- Under these conditions, equivalent roughness and waviness parameters arising from the motif characterization method (R_{eq}, W_{eq}, AR_{eq}, AW_{eq}) appeared to have no correlation with the interfacial breakdown strength alone. However, a negative correlation between the estimated

equivalent asperity aspect ratio, R_{eq}/β_{eq} , and the breakdown strength was observed over all tests.

- It is suggested that at low contact force, the asperity radii have a stronger effect in determining interfacial breakdown, since the surfaces are not compressed with sufficient force to cause significant deformation of surface asperities therefore forming strong contact spots. As a result, the field enhancement at the interface is determined by the size and radius of the asperities – the higher the asperity aspect ratio, the higher the degree of field enhancement, and the lower the interfacial breakdown strength.
- The above point appears to be supported by the much-reduced interfacial breakdown strength of Ultem interfaces. The asperity aspect ratio of Ultem interfaces was among the highest of all tested interfaces, suggesting the existence of sharper and higher aspect ratio asperities at the contact. The reason is believed to be linked to the brittleness of Ultem compared to all other materials, which can be inferred from its Charpy impact strength that is 3–4 times lower than all other materials used in this work. Local brittle fracture during machining is then thought to explain the sharper surface features, leading to reduced interfacial breakdown strength.
- Inspection of post-breakdown traces left by the plasma breakdown channels indicate that under 2400 kV/µs pulses, a single, central, breakdown channel was far more likely to result after repeated breakdown events. In contrast, under 0.35 kV/µs pulses, multiple different (longer) discharge paths were taken, some of which originate from the edges of the electrode rather than down the center (i.e., critical path considering only the Laplacian field).
- It is believed that the additional time available during 0.35 kV/µs pulses allows sufficient space charge transport prior to breakdown that modifies the field distribution, which may explain the redirection of the breakdown path as the electric field is distorted from the Laplacian state near the needle tip.
- As a result, the average of the widths of the breakdown-affected region at the interfaces were found to be wider for the 0.35 kV/µs case, being on average about twice as wide as those in the 2400 kV/µs case.

The results presented in this work further emphasizes the necessity to maintain mating pressure where solid interfaces cannot be avoided, as its reduction may lead to the weakening of the dielectric strength below that of pure gas insulation, risking catastrophic failure. They further indicate that under conditions like those studied in this work, the roughness and waviness parameters alone may play less of a role in the determination of interfacial breakdown voltage, since discharges can readily form and propagate with little to impede them. The analyses conducted here also suggest (depending on how materials are cut or treated) the possibility that material brittleness plays a role in determining the aspect ratio of surface asperities, which under low mating pressure, appears important for interfacial breakdown. Given that in many applications, no specific treatment will be used to attain specific surface roughness conditions prior to mating, this work may provide additional information for appropriate material selection for the design of HV pulsed power insulating systems. The differences in the post-breakdown channel width may further be of critical importance for compact pulsed system design, as the effective width of the discharge region has shown to be dependent on the pulse rise time and on the interface material.

Several aspects identified from this work remain to be addressed. These include:

- The effect of *dV/dt* on the critical distance, where positive and negative breakdown voltages are the same, as observed in the present electrode topology.
- The effect of the inclusion of a solid interface on the critical distance – does such a parameter even exist for solid-solid interfacial breakdown?
- Why does Delrin develop an abnormally wide post-breakdown region under the 2400 kV/µs case, behavior which differs from all other materials?
- More conclusive confirmation of the effects of material brittleness, perhaps from more detailed analysis of the freshly-cut surface morphologies, or from a more detailed and quantitative measure of brittleness via stress-strain curves.
- Expanded study to include more materials, different values of *dV/dt*, and further investigation into the role of contact pressure.

ACKNOWLEDGMENTS

The authors would take this opportunity to gratefully acknowledge Andrew Carlin, Seak Doak, and Louis Cooper, for their aid in test-cell fabrication and sample preparation.

REFERENCES

[1] C. Zhang, X. Lyu, N. Arshad, R. M. Aadil, Y. Tong, W. Zhao, and R. Yang, "Pulsed electric field as a promising technology for solid foods processing: A review," *Food Chem.*, vol. 403, no. 134367, Mar. 2023.

[2] S. H. Jayaram, A. H. El-Hag, F. P. Espino-Cortes, R. J. Wong and C. Leibovitch, "Effects of process and product parameters on the shape of nanosecond pulses used in high-field liquid food treatment," *IEEE Trans. Ind. Appl.*, vol. 41, no. 2, pp. 520-526, Apr. 2005.

[3] C.-M. Liu, Y. Nishida, K. Iawsaki, W. Sung and F.-P. Wu, "Characteristics of DC or Pulsed-Type High-Electric Field Plasma and its Application to Air Cleaning System," *IEEE Trans. Plasma Sci.*, vol. 2, no. 47, pp. 1121-1128, Feb. 2019.

[4] Y. Guo *et al.*, "Enhancing PM Removal by Pulse Energized Electrostatic Precipitators-a Comparative Study," *IEEE Trans. Plasma Sci.*, vol. 47, no. 1, pp. 365-375, Jan. 2019.

[5] D. Kaushik and M. J. Thomas, "Design of Pulse Forming Systems for Pulsed Electromagnetic Manufacturing Applications," *IEEE Trans. Plasma Sci.*, vol. 50, no. 10, pp. 3677-3684, Sep. 2022.

[6] S. Okabe, T. Tsuboi and J. Takami, "Basic study of possible waveforms generated in lightning impulse withstand voltage test on UHV equipment," *IEEE Trans. Dielectr. Electr. Insul.*, vol. 16, no. 4, pp. 1127-1133, Aug. 2009.

[7] M. Li, Z. Wang, R. Xu, X. Zhang, Z. Chen and Q. Wang, "Advances in plasma-assisted ignition and combustion for combustors of aerospace engines," *Aerosp. Sci. Technol.*, vol. 117, no. 106952, Oct. 2011.

[8] T. A. Mehlhorn, "National Security Research in Plasma Physics and Pulsed Power: Past, Present, and Future," *IEEE Trans. Plasma Sci.*, vol. 42, no. 5, pp. 1088-1117, May 2014.

[9] T. Takahashi, T. Okamoto, Y. Ohki and K. Shibata, "Breakdown strength at the interface between epoxy resin and silicone rubber-a basic study for the development of all solid insulation," *IEEE Trans. Dielectr. Electr. Insul.*, vol. 12, no. 4, pp. 719-724, Aug. 2005.

[10] D. Fournier and L. Lamarre, "Effect of pressure and length on interfacial breakdown between two dielectric surfaces," in *Conf. Rec. 1992 IEEE Int. Symp. Electr. Insul.*, Baltimore, MD, USA, Jun. 1992.
[11] D. Fournier, C. Dang and L. Paquin, "Interfacial breakdown in cable joints," in *Proc. 1994 IEEE Int. Symp. Electr. Insul.*, Pittsburgh, PA, USA, Jun. 1994.
[12] R. Ross, "Dealing with interface problems in polymer cable terminations," *IEEE Electr. Insul. Mag.*, vol. 15, no. 4, pp. 5-9, Jul. 1999.
[13] B. X. Du and L. Gu, "Effects of interfacial pressure on tracking failure between XLPE and silicon rubber," *IEEE Trans. Dielectr. Electr. Insul.*, vol. 17, no. 6, pp. 1922-1930, Dec. 2020.
[14] S. M. Hasheminezhad, E. Ildstad and A. Nysveen, "Breakdown strength of solid—solid interface," in *10th IEEE Int. Conf. Solid Dielectr.*, Potsdam, Germany, Jul. 2010.
[15] M. Hasheminezhad and E. Ildstad, "Application of contact analysis on the evaluation of breakdown strength and PD inception strength of solid-solid interfaces," *IEEE Trans. Dielectr. Electr. Insul.*, vol. 19, no. 1, pp. 1-7, Feb. 2012.
[16] E. Kantar, D. Panagiotopoulos and E. Ildstad, "Factors influencing the tangential AC breakdown strength of solid-solid interfaces," *IEEE Trans. Dielectr. Electr. Insul.*, vol. 23, no. 3, pp. 1778-1788, Jun. 2016.
[17] E. Kantar, F. Mauseth, E. Ildstad and S. Hvidsten, "Longitudinal AC breakdown voltage of XLPE-XLPE interfaces considering surface roughness and pressure," *IEEE Trans. Dielectr. Electr. Insul.*, vol. 24, no. 5, pp. 2047-2054, Oct. 2017.
[18] E. Kantar, E. Ildstad and S. Hvidsten, "Effect of material elasticity on the longitudinal AC breakdown strength of solid-solid interfaces," *IEEE Trans. Dielectr. Electr. Insul.*, vol. 26, no. 2, pp. 655-663, Mar. 2019.
[19] E. Kantar, E. Ildstad and S. Hvidsten, "Effect of elastic modulus on the tangential AC breakdown strength of polymer interfaces," *IEEE Trans. Dielectr. Electr. Insul.*, vol. 26, no. 1, pp. 211-219, Jan. 2019.
[20] E. Kantar, S. Hvidsten, F. Mauseth and E. Ildstad, "A stochastic model for contact surfaces at polymer interfaces subjected to an electrical field," *Tribol. Int.*, vol. 127, pp. 361-371, Nov. 2018.
[21] E. Kantar, S. Hvidsten, F. Mauseth and E. Ildstad, "A deterministic breakdown model for dielectric interfaces subjected to tangential electric field," *J. Phys. D: Appl. Phys.*, vol. 54, no. 29, p. 295503, May 2021.
[22] I. C. Somerville, S. J. MacGregor and O. Farish, "An efficient stacked-Blumlein HV pulse generator," *Meas. Sci. Technol.*, vol. 1, no. 9, pp. 865-868, Apr. 1990.
[23] *Geometrical Product Specifications (GPS) - Surface texture: Profile method - Motif parameters ISO 12095, 1996*.
[24] S. Belghith, S. Mezlini, H. BelhadjSalah and J.-L. Ligier, "Modeling of contact between rough surfaces using homogenisation technique," *Comptes Rendus Mécanique*, vol. 338, no. 1, pp. 48-61, Jan. 2010.
[25] M. G. Hogg, I. V. Timoshkin, S. J. MacGregor, M. P. Wilson and M. J. Given, "Polarity effects on breakdown of short gaps in a point-plane topology in air," *IEEE Trans. Dielectr. Electr. Insul.*, vol. 22, no. 4, pp. 1815-1822, Aug. 2015.
[26] L. Zhao, J. Su, X. Zhang, and Y. Pan, "Experimental investigation on the role of electrodes in solid dielectric breakdown under nanosecond pulses," *IEEE Trans. Dielectr. Electr. Insul.*, vol. 19, no. 4, pp. 1101-1107, Aug. 2012.
[27] L. Zhao, G. Liu, J. Su, Y. Pan, and X. Zhang, "Investigation of Thickness Effect on Electric Breakdown Strength of Polymers Under Nanosecond Pulses," *IEEE Trans. Plasma Sci.*, vol. 39, no. 7, pp. 1613-1618, Jul. 2011.
[28] J. A. Greenwood and J. B. P. Williamson, "Contact of nominally flat surfaces," *Proc. R. Soc. Lond. A Math. Phys. Sci.*, vol. 295, no. 1442, pp. 300-319, Dec. 1966.
[29] F. Robbe-Valloire, "Statistical analysis of asperities on a rough surface," *Wear*, vol. 249, no. 5-6, pp. 401-408, Jun. 2001.
[30] *Plastics - Determination of Charpy impact properties - Part 1: Non-instrumented impact test ISO 179-1, 2010*.

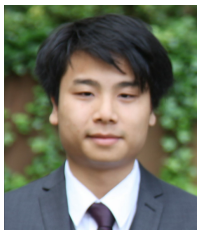

Timothy Wong (Graduate Student Member, IEEE) received the M.Eng degree in electrical and mechanical engineering with international study from The University of Strathclyde, Glasgow, U.K., in 2020. He is currently pursuing the degree of Ph.D. in electronic and electrical engineering at the University of Strathclyde, Glasgow, U.K., with the High Voltage Technologies research group. His current research interests include the pulsed breakdown of solid-solid dielectric interfaces, solid-gas interfaces, computational modelling of fast ionisation fronts and streamer discharges in gas and gas-solid topologies, and pulsed power insulation system design. He was the recipient of the IMechE student award in 2020 where he is an Associate Member; and is currently a graduate student member of the IEEE Dielectrics and Electrical Insulation society (DEIS) and the IEEE Nuclear and Plasma Sciences society (NPSS). He is also a member of the IET. He was the recipient of the DEIS Best Student Presentation Award at the 14th Universities High Voltage Network Colloquium in 2022 and was further awarded the NPSS Outstanding Student Paper Award at the 24th IEEE International Pulsed Power Conference in 2023.

Igor Timoshkin (Senior Member, IEEE) received the degree in physics from Moscow State University, Moscow, Russia, in 1992, and the Ph.D. degree from the Imperial College of Science, Technology, and Medicine (ICSTM), London, U.K., in 2001. He was a researcher at Moscow State Agro Engineering University, Moscow, and then at the Institute for High Temperatures of Russian Academy of Sciences, Moscow. In 1997 he joined ICSTM. Then he joined the department of Electronic and Electrical Engineering, University of Strathclyde, Glasgow, U.K., in 2001, where he became a Reader in 2016. His research interests include dielectric materials, pulsed power, transient spark discharges, environmental applications of non-thermal plasma discharges. Dr. Timoshkin was a Voting Member of the Pulsed Power Science and Technology Committee in the IEEE Nuclear and Plasma Science Society (2017-2021); currently he is a member of International Advisory Committee of the IEEE Conference on Dielectric Liquids, a member of the International Scientific Committee of the Gas Discharges and Their Applications Conference, and a Subject Editor of IET Nanodielectrics.

Scott MacGregor (Senior Member, IEEE) received the B.Sc. and Ph.D. degrees from the University of Strathclyde, Glasgow, U.K., in 1982 and 1986, respectively. He was a Pulsed-Power Research Fellow in 1986 and a Lecturer in pulsed-power technology in 1989. In 1994, he became a Senior Lecturer, with a promotion to Reader and a Professor of High Voltage Engineering, in 1999 and 2001, respectively. In 2006 and 2010, he became the Head of the Department of Electronic and Electrical Engineering and the Executive Dean of the Faculty of Engineering, and has been the Vice-Principal with the University of Strathclyde, since 2014. His current research interests include high-voltage pulse generation, high-frequency diagnostics, highpower repetitive switching, high-speed switching, electronic methods for food pasteurization and sterilization, the generation of high-power ultrasound (HPU), plasma channel drilling, pulsed-plasma cleaning of pipes, and the stimulation of oil wells with HPU. Prof. MacGregor was a recipient of the 2013 IEEE Peter Haas Award. He was an Associated Editor of the IEEE Transactions of Dielectrics and Electrical Insulation in 2015.

Mark Wilson (Member, IEEE) was born in Stranraer, Scotland, in 1982. He received the B.Eng. (with honours), M.Phil., and Ph.D. degrees in electronic and electrical engineering from the University of Strathclyde, Glasgow, U.K., in 2004, 2007, and 2011, respectively. He is presently based in the High Voltage Technologies research group at the University of Strathclyde, where his research interests include interfacial surface flashover, nanodielectrics, and the practical applications of high-power ultrasound, corona discharges, and pulsed electric fields. Mark is a member of the IEEE Nuclear and Plasma Science Society, from whom he received a Graduate Scholarship Award in 2011, the IEEE Dielectrics and Electrical Insulation Society, and the IET.

Martin Given (Senior Member, IEEE) received the B.Sc. degree in physics from the University of Sussex, Brighton, U.K., in 1981, and the Ph.D. degree in electronic and electrical engineering from the University of Strathclyde, Glasgow, U.K., in 1996. He is currently a Senior Lecturer with the Department of Electronic and Electrical Engineering, University of Strathclyde. His current research interests include ageing processes and condition monitoring in solid and liquid insulation systems, highspeed switching, and pulsed power.